2017 American Control Conference
Sheraton Seattle Hotel
May 24–26, 2017, Seattle, USA

Combustion Shaping Using Multivariable Feedback Control*

Bryan P. Maldonado[1], Huan Lian[1], Jason B. Martz[1], Anna G. Stefanopoulou[1],
Kevin Zaseck[2], Eiki Kitagawa[2]

***Abstract*— As high exhaust gas recirculation (EGR) is introduced for efficiency, the combustion duration and combustion delay is elongated due to slow fuel burn rates requiring flexible and robust management of both the combustion initiation and duration (what we call *combustion shaping*). Combustion shaping through cylinder pressure sensing and feedback control of spark advance (SA) and EGR-valve position can be used for spark ignited (SI) engines operating within highly dilute, high efficiency regimes even where the combustion variability (CV) limits controller bandwidth. Although EGR is directly related with combustion duration, spark advance affects the start and duration of combustion simultaneously. This input/output coupling suggests a multivariable controller that coordinates the actuators. Control of SA and EGR is investigated with a coupled linear quadratic Gaussian (LQG) controller and compared with a decoupled proportional-integral (PI) controller. Simulation of the closed-loop system uses a simple engine model derived from system identification. Gain tuning was performed aiming for fast response without overshoot and considering cyclic variability reduction through a Kalman filter. Comparison of the simulated controllers shows that the LQG controller has better transients and responds better to CV.**

I. INTRODUCTION

Combustion phasing or the crank angle where 50% of fuel is burned (CA50) is an important engine performance metric based on which the spark advance (SA) is tuned and its values are stored in a lookup table. A knock sensor is used to retard the spark timing when knock is detected [1]. Research in closed-loop combustion control for maintaining a desirable combustion phasing despite small mixture (fuel, air, or dilution) variations has been also studied using cylinder pressure ([2]) or ion-sensing ([3]). This work presents an effort to enhance the closed-loop control of the combustion phasing, by controlling both the start of combustion (crank angle where 10% of fuel is burned) and the combustion duration (crank angle degrees between the 10% and 90% of fuel burned). This enhancement might be necessary in the future due to the need for increased combustion dilution.

The use of external exhaust gas recirculation (EGR) in stoichiometric spark-ignited (SI) engines improves fuel economy by reducing pumping work and heat transfer losses [4]. However, fuel burn rates decrease with EGR, causing longer combustion duration. Advancing spark could shift the combustion center towards the target values, but high SA can reach the misfire limit before reaching the maximum brake torque (MBT) value [5]. For this reason, the initiation and duration of combustion need to be managed within a desirable range [3]. Previous studies have maintained SI combustion phasing through closed-loop SA control, while combustion duration was controlled via lookup table based EGR scheduling [6], [3]. However such open-loop approaches are vulnerable to uncertainties due to environmental factors (altitude, humidity, temperature) or EGR system aging effects. The problem with combustion feedback rises when the controller responds to the combustion variability (CV) and can cause closed-loop cyclic variability higher than the open-loop CV.

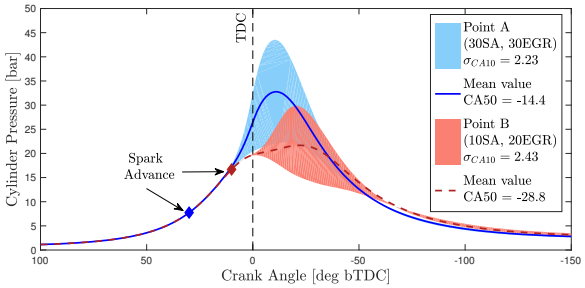

Fig. 1. Pressure trace corresponding to 2000 cycles at different EGR levels and spark advances at the same speed (1600 [RPM]) and load (50 [N-m]).

This paper attempts to overcome these limitations by investigating the closed-loop control of *combustion shaping*, where combustion start and duration are controlled by a multiple-input multiple-output (MIMO) controller of SA and EGR-valve position. We discuss the controller design given the coupling between the combustion features (start and duration) and the control inputs. Specifically, the paper develops, analyzes, and compares a decentralized PI controller and a centralized linear quadratic Gaussian (LQG) controller with respect to their ability to achieve combustion shaping by independently controlling the two combustion features. Adequate and fast control of transients is also sought, given that a) the inherent coupling of combustion start and duration may lead to undesirable transient behaviors, such as long combustion duration with a late start that results in misfire and b) the high CV that can inhibit high bandwidth feedback.

This paper is organized as follows: Section II shows the combustion features statistics for the engine. Section III explains the system identification steps at various operating points. In Section IV a linear analysis of the input/output system is performed for control design in Section V, based on the combustion behavior of the operating conditions shown in Fig. 1. Finally, Section VI compares the coupled and decoupled controllers both in time and frequency domain.

*This work was supported by Toyota Motor Corporation

[1]Department of Mechanical Engineering, University of Michigan. 1231 Beal Ave. Ann Arbor, Michigan 48109 bryanpm@umich.edu

[2]Toyota Motor Engineering & Manufacturing North America, Inc. 1555 Woodridge Ave. Ann Arbor, Michigan 48105 kevin.zaseck@toyota.com

II. EXPERIMENTAL SETUP

A. Engine Characteristics

A production 1.3 L, gasoline fueled Toyota 1NR-FKE engine is used in this study. The four-cylinder, SI engine is port fuel injected, throttled, and uses water cooled EGR [7]. The combustion chamber has the following characteristics:

- Compression Ratio: 13.5
- Stroke: 80.5 [mm]
- Displacement: 1329 [cc]
- Bore: 72.5 [mm]

This production engine is mainly used for the Toyota Ractis 120, Toyota Vitz 130, and Subaru Trezia, and is equipped with in-cylinder pressure sensors for this work. Heat release analysis with data from these transducers is used to compute the following combustion features at every cycle:

CA10: Crank angle when 10% of the fuel mass is burned (associated with combustion start)

CA50: Crank angle when 50% of the fuel mass is burned (associated with combustion center)

CA1090: Duration in crank angle degrees between when 10% and 90% of the fuel mass is burned

For this study, a dynamometer regulated the engine speed to 1600 [RPM]. At each condition we altered throttle to maintain an engine torque at 50 [N-m].

B. Steady State Values

Tables I and II respectively present the combustion start and duration mean values (in black) and standard deviation (in blue) for the range of EGR and SA investigated in this work. The statistics were calculated using 2000 cycles at steady state. Figure 1 shows the pressure trace of the two operating points shown in bold. Points that do not contain data correspond to regions where engine operation is problematic due to knock, misfire and slow burns.

III. SYSTEM IDENTIFICATION

Combustion models were created by performing step changes in EGR and SA and fitting the CA10 and CA1090 response with low order input-output dynamic models to assist with control development. Figure 2 shows that increasing EGR delays ignition and lengthens combustion duration. Whereas, advancing spark starts combustion earlier and shortens the duration. The measured values were filtered using Savitzky-Golay finite-impulse response (FIR) smoothing filter [8]. Given the sharp slope in Fig. 2 after the step and the lack of significant overshoot in the filtered response, a first order dynamical model is deemed appropriate for control analysis and design.

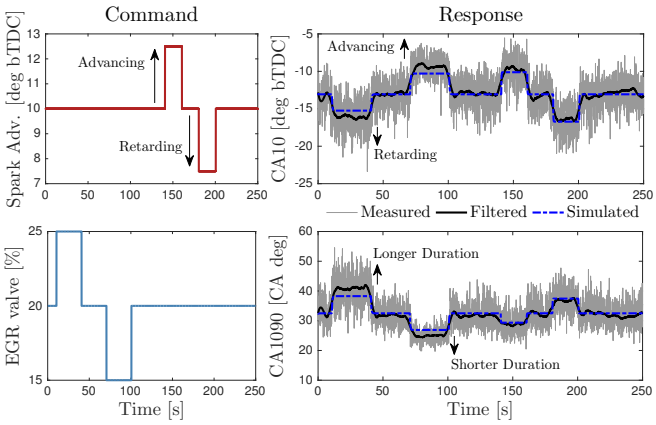

Fig. 2. CA10 and CA1090 responses to step commands around the operating condition SA = 10 [deg bTDC] and EGR = 20% valve opening. Simulated data was obtained using the model described in Section III-C

A. First Order Discrete Model

A single-input single-output (SISO) first order discrete dynamic system can be represented by the difference equation:

$$\hat{y}[k+1] = (1-a)\hat{y}[k] + (K_{DC}a)u[k]. \tag{1}$$

Where $\hat{y}$ is the estimated output, K_{DC} is the DC gain, and $a = T/\tau$, where τ is the time constant and T the time interval at which the engine control unit (ECU) updates. The DC gain is calculated as the ratio between the output change and the corresponding command change as follows:

$$K_{DC} = \frac{\Delta y}{\Delta u} = \frac{\bar{y}_{\text{fin}} - \bar{y}_{\text{ini}}}{u_{\text{fin}} - u_{\text{ini}}}. \tag{2}$$

The variable $\bar{y}$ denotes the measured average output value at steady state before ($\bar{y}_{\text{ini}}$) and after ($\bar{y}_{\text{fin}}$) the step. $\bar{y}_{\text{ini}}$ was calculated using 50 cycles prior to the step while for $\bar{y}_{\text{fin}}$ the values between the 50th and 100th cycle after the step were used. Defining the residual between the model and the measured values as $R(a) = |\hat{y}(a) - y|$, the objective function $R(a)$ was minimized subject to the open loop stability condition as follows:

$$\min_a R(a), \text{ such that: } 0 < a \leqslant 1. \tag{3}$$

TABLE I

VALUES OF CA10 [deg bTDC]: Averages and Standard Deviations

EGR valve opening		Spark Advance [deg bTDC] 5	10	15	20	25	30	35	40	45
10%	KNOCK	-13.12 (2.14)	-6.77 (1.81)	-1.47 (1.59)						
20%	KNOCK	-18.31 (2.59)	**-13.03 (2.43)**	-8.43 (2.28)	-4.33 (2.23)	-0.23 (2.06)	3.26 (1.97)		MISFIRE	
30%				-10.17 (2.42)	-6.38 (2.32)	-3.72 (2.35)	**-0.41 (2.23)**	2.16 (2.32)		
40%		MISFIRE / SLOW BURN				-5.78 (2.48)	-2.91 (2.40)	-1.23 (2.59)	0.89 (2.91)	2.49 (3.73)

() = Standard deviation: σ_{CA10}

TABLE II

VALUES OF CA1090 [CA deg]: Averages and Standard Deviations

EGR valve opening		Spark Advance [deg bTDC] 5	10	15	20	25	30	35	40	45
10%	KNOCK	24.69 (2.15)	21.12 (1.72)	18.84 (1.58)						
20%	KNOCK	35.67 (4.26)	**32.18 (4.14)**	29.44 (3.65)	24.93 (3.34)	24.47 (2.98)	22.98 (2.64)		MISFIRE	
30%				33.35 (4.54)	31.14 (4.26)	30.53 (4.20)	**28.23 (3.92)**	27.10 (3.71)		
40%		MISFIRE / SLOW BURN				33.66 (4.86)	31.42 (4.38)	30.72 (4.32)	29.90 (4.28)	29.54 (4.65)

() = Standard deviation: σ_{CA1090}

B. Operating Conditions

To analyze and develop the combustion shaping controller, steps were performed between the two conditions highlighted in Fig. 1 and Tables I and II. We refer to them as:

- POINT A: $(\text{SA} = 30, \text{EGR} = 30)$
  $(\text{CA10} = 0,\ \text{CA50} = -14.4,\ \text{CA1090} = 28)$
  $(\sigma_{\text{CA10}} = 2.23,\ \sigma_{\text{CA50}} = 3.59,\ \sigma_{\text{CA1090}} = 3.92)$
- POINT B: $(\text{SA} = 10, \text{EGR} = 20)$
  $(\text{CA10} = -13,\ \text{CA50} = -28.8,\ \text{CA1090} = 32)$
  $(\sigma_{\text{CA10}} = 2.43,\ \sigma_{\text{CA50}} = 3.30,\ \sigma_{\text{CA1090}} = 4.14)$

We chose these two points to simplify the analysis due to the similarity between the time constants of the first order model, along with the similar standard deviation of both CA10 and CA1090. Future work will investigate extensions to operating points with different dynamics and different CV levels. In both cases, the system response to SA corresponded to $\tau_{SA} = 0.17$ [sec], while for EGR $\tau_{EGR} = 0.40$ [sec]. Although different gains and time constants were identified in upward and downward steps and in various operating SA and EGR levels, a representative time constant was used for both combustion features in response to a step in SA. Similarly, one average time constant across all points in Tables I and II was used for changes in EGR.

C. Engine Model

Figure 3 shows the block diagram of the model used for simulation. The engine inputs are fed to the transfer function corresponding to a first order discrete dynamic system with unity gain and fixed time constant (either τ_{SA} or τ_{EGR}). The DC gain values are given by a fourth order polynomial interpolation of the values in Tables I and II. This model is limited to the given speed-load condition, different combinations will require a different combustion model.

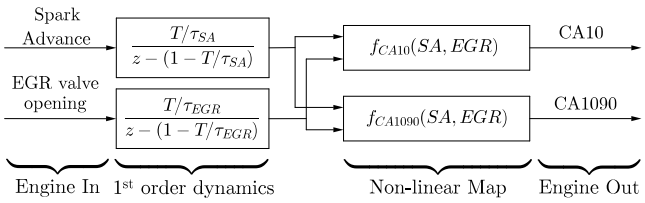

Fig. 3. Engine model used for simulation.

IV. COUPLING ANALYSIS

As physics dictate, SA and EGR affect both CA10 and CA1090 creating a coupled two-input two-output system. To achieve satisfactory control it is important to determine the feasible range over which SA and EGR can effectively manipulate CA10 and CA1090. Given the strong coupling between SA and start of combustion, intuition suggests using a PI controller to track CA10 set points using SA. Due to the time constant separation, it is also feasible to use the EGR command to reject the effect of SA on CA1090, and regulate or track CA1090 to its desired value using another PI controller. However, the second PI controller might not be able to completely reject the SA command since high PI gains increase the CV in the closed loop system. Thus, a coordinated multivariable feedback controller can achieve a better response. The following sections will determine if (a) the decentralized structure described earlier can be improved by a multivariable design and (b) if the multivariable controller will sustain its benefits despite the high CV.

A. DC Gain Matrix

The DC gain can point to the combinations of combustion start and duration (CA10 and CA1090) that will require high actuator action and hence are less feasible than others [9]. Let $\boldsymbol{K_{DC}}$ be the DC gain matrix that maps actuator commands into steady state combustion phasing values as follows:

$$\begin{bmatrix} \delta\text{CA10} \\ \delta\text{CA1090} \end{bmatrix} = \boldsymbol{K_{DC}} \begin{bmatrix} \delta\text{SA} \\ \delta\text{EGR} \end{bmatrix} \tag{4}$$

Table III summarizes the properties of $\boldsymbol{K_{DC}}$ for POINTS A and B. Note that neither of the two matrices are diagonally dominant, meaning that a *coupled* multivariable controller is necessary to coordinate the two actuators and fully utilize their joint effect on combustion shaping. Nonetheless, we still analyze the decoupled PI controller for comparison.

TABLE III
DC GAIN MATRIX PROPERTIES

POINT A	POINT B
$\boldsymbol{K_{DC}} = \begin{bmatrix} 0.55 & -0.51 \\ -0.48 & 1.03 \end{bmatrix}$	$\boldsymbol{K_{DC}} = \begin{bmatrix} 1.36 & -0.62 \\ -1.61 & 1.46 \end{bmatrix}$
$\det = 0.32$	$\det = 0.98$
$\kappa = 5.56$	$\kappa = 6.93$
$\sigma_{\min} = 0.24$	$\sigma_{\min} = 0.38$
$\sigma_{\max} = 1.34$	$\sigma_{\max} = 2.61$
$\text{RGA}_{(1,1)} = \text{RGA}_{(2,2)} = 1.76$	$\text{RGA}_{(1,1)} = \text{RGA}_{(2,2)} = 2.01$

$\det$ = determinant $\kappa = \sigma_{\max}/\sigma_{\min}$ = condition number
σ = singular value

In order to decide an input-to-output pairing for the decentralized control architecture, we will use the relative gain array (RGA) approach [10], [11]. The RGA for both matrices has positive diagonal entries, suggesting the pairing of CA10 with SA and CA1090 with EGR. From a physical point of view, EGR can directly increase CA1090 duration by slowing the combustion process at high dilution.

Investigation of the coupled characteristics is also needed for establishing feasibility conditions for MIMO integral control. In other words, $\boldsymbol{K_{DC}}$ cannot be ill-conditioned and its inverse must exist to allow the augmentation of integrator states involving the two combustion features we wish to control [12]. The condition number (κ) is similar for both matrices and is on the order of 1, meaning that the control problem of tracking two outputs (CA10 and CA1090) with two inputs (SA and EGR) is well conditioned and the integral controller can manage both modeling error and disturbances well. Neither DC gain matrix determinant is close to zero, so the inverse matrix should be robust to feedback signal variability. However, the determinant at POINT B is almost one, so CV will not amplify actuator commands considerably. Due to this property, $\boldsymbol{K_{DC}}$ at POINT B will be used for tuning the feedback and observer gains of the LQG controller.

V. CONTROL DESIGN

An LQG controller will be designed given the interaction between input/output engine variables. Moreover, using a Kalman filter will aid in the reduction of CV observed under these highly diluted conditions. Two separate PI controllers are also simulated for comparison due to their intuitive structure and ease of implementation. The dynamic model with the nonlinear map provides a surrogate model for evaluating the closed-loop behavior before implementation.

A. PI controller

Consider the decoupled control architecture depicted in Fig. 4. Each actuator is driven by a SISO PI controller.

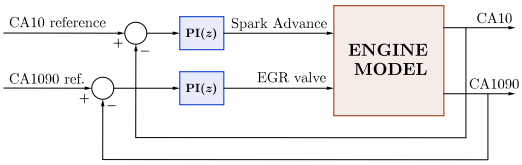

Fig. 4. Decoupled PI controllers.

Controller gains are tuned using the sequential loop closing technique, closing the spark loop first since it has the fastest time constant [13]. When the spark loop is closed, gains are chosen to accomplish a fast settling-time while avoiding overshoot in CA10 simultaneously. When we closed the second loop, controller gains are chosen to also minimize CA1090 overshoot, without harming the previous loop performance. Table IV summarizes the gain values selected.

TABLE IV
PI GAIN VALUES

Controller	Spark Advance	EGR valve
P: Proportional	0.5	0.1
I: Integral	0.1725	0.195

B. Linear Quadratic Gaussian controller

Consider the MIMO controller described by Fig. 5. The engine states are estimated using the infinite horizon linear quadratic estimator (LQE) technique. Note that estimation is not necessary for the integrator states [12]. Since the measurements of the combustion features vary from cycle-to-cycle mostly due to the process, pressure sensor, and electronics noise, the Kalman filter will reduce this variability from the engine estimated states. The measurements however are not filtered before input into to the integrator. The linear time-invariant model described in Section IV with the states corresponding to the SA and EGR dynamics together with the disturbance and noise signals are considered:

$$\begin{aligned} x[k+1] &= Ax[k] + B(u[k] + w[k]) \\ y[k] &= Cx[k] + v[k] \end{aligned} \tag{5}$$

where $w[k], v[k]$ are wide sense stationary, zero mean, Gaussian processes (white noise) with covariance kernels W, V respectively. The observer will have the form of a discrete-time delayed Kalman estimator, i.e. using measurements up to $y[k-1]$ [14]. The covariance matrix V can be estimated from the measured steady state signals shown in Tables I and II. Using the range of the observed CV for $\sigma_{\text{CA10}} \in [1.59, 3.73]$ and $\sigma_{\text{CA1090}} \in [1.58, 4.86]$, the average standard deviation of all operating conditions was calculated to estimate the measurement covariance:

$$\begin{aligned} V_{\text{CA10}} &= 2.3^2 \ [\text{deg}^2] \\ V_{\text{CA1090}} &= 4^2 \ [\text{deg}^2]. \end{aligned} \tag{6}$$

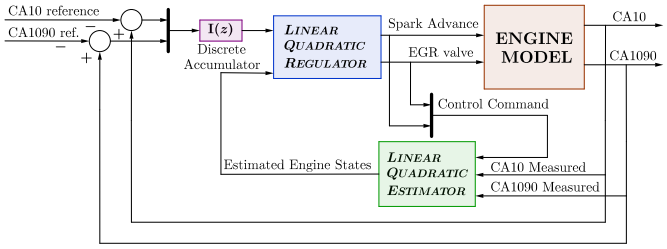

Fig. 5. Coupled LQG controller.

The covariance kernels of the LQE are the following diagonal positive definite matrices:

$$V = \text{diag}\begin{pmatrix} V_{\text{CA10}} & V_{\text{CA1090}} \end{pmatrix}, W = \text{diag}\begin{pmatrix} W_{\text{CA10}} & W_{\text{CA1090}} \end{pmatrix}. \tag{7}$$

Since V is already given by experimental data, matrix W is used to tune the observer gain. The following diagonal values were used based on the variability reduction for engine estimated states in simulations:

$$W_{\text{CA10}} = W_{\text{CA1090}} = 0.1. \tag{8}$$

Consider the discrete state feedback controller with augmented integrators:

$$u[k] = -K\begin{bmatrix} \hat{x}[k] & x_I[k] \end{bmatrix}^T. \tag{9}$$

Where $\hat{x}[k]$ are the estimated engine states and $x_I[k]$ are the the integrator states. The augmented discrete system has the form:

$$\begin{bmatrix} x[k+1] \\ x_I[k+1] \end{bmatrix} = \underbrace{\begin{bmatrix} A & 0 \\ C & I \end{bmatrix}}_{A_{\text{aug}}} \begin{bmatrix} x[k] \\ x_I[k] \end{bmatrix} + \underbrace{\begin{bmatrix} B \\ 0 \end{bmatrix}}_{B_{\text{aug}}} u[k] + \begin{bmatrix} 0 \\ -I \end{bmatrix} r[k]. \tag{10}$$

Given that the pair $(A_{\text{aug}}, B_{\text{aug}})$ is controllable, the optimal cost of the infinite horizon linear quadratic regulator (LQR) is finite [12]. Since the model states do not have physical measurement, we use a diagonal positive definite weighting matrix for the system output as follows:

$$Q' = \text{diag}(Q_{\text{CA10}},\ Q_{\text{CA1090}},\ Q_{\int \text{CA10}},\ Q_{\int \text{CA1090}}). \tag{11}$$

Hence, the weighting matrix for the engine states is $Q = C_{\text{aug}}^T Q' C_{\text{aug}}$. Given that the pair $(A_{\text{aug}}, \sqrt{Q})$ is detectable, the optimal state feedback stabilizes the system [12]. The positive definite weighting matrix that penalizes the control signal is given by:

$$R = \text{diag}(R_{SA},\ R_{EGR}). \tag{12}$$

Table V summarizes the costs used in the weighting matrix for the LQR. Tuning was performed manually, aiming for a fast rise-time and avoiding overshoot.

TABLE V

DIAGONAL VALUES FOR LQR WEIGHTING MATRICES

Cost	System output: Q'				Control: R	
	Q_{CA10}	Q_{CA1090}	$Q_{\int \text{CA10}}$	$Q_{\int \text{CA1090}}$	R_{SA}	R_{EGR}
LQR	5	5	0.6	0.4	5	5

VI. RESPONSE COMPARISON

The above controllers are compared here in time and frequency domains. The closed-loop response of the system is analyzed in time domain based on rise-time, settling-time and overshoot performance. Feedback and closed-loop transfer functions are analyzed in frequency domain via Bode magnitude plots. Additionally, white noise is introduced in the simulations based on the variability corresponding to the observed engine output at POINT A and POINT B.

A. Time Domain

The engine response and actuator effort of both controllers for step commands between POINT A and POINT B are shown in Fig. 6 and 7. In particular, Fig. 7 includes simulated measurement noise to compare variability between the controllers. Tables VI and VII summarize the time domain performance values of the different closed loop systems. Symbolic qualitative comparison is given for a quick assessment, based on a relative evaluation between controllers. Here, *rise-time* is defined as the time between 0% to 90% of the step magnitude, *settling-time* is defined as the time until the output reaches the error band $\pm 5\%$ of the target value, and *overshoot* is the maximum peak exceeding the final value, with respect to the step direction. Overshoot percentage is relative to the step magnitude.

Overshoot in CA1090 for the PI controller is due to the influence of spark on both outputs. In the LQG case, overshoot in CA1090 is almost nonexistent thanks to the coordinated effort of both actuators. However, rise-time in CA1090 is longer than the one for the PI controller. Recall that a long combustion duration will increase variability and will adversely affect the benefits of EGR. Therefore, overshoot in the POINT A → POINT B step is undesirable. Note how similar the responses of CA10 are for both controllers, but they differ considerably in CA1090 response. This is due to the sequential loop closing procedure, since the first loop (spark loop) was tuned based on time domain constraints (fast settling and no overshoot) which coincides with the LQG controller constraints. The second loop (EGR loop) cannot achieve the same requirements since the first loop

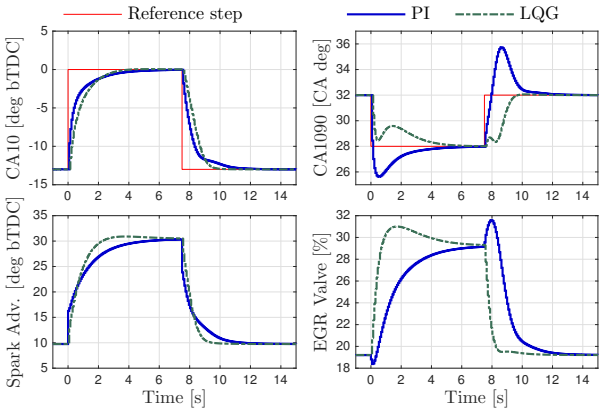

Fig. 6. Simulated comparison for step POINT B → POINT A → POINT B using the nonlinear model of Section III-C.

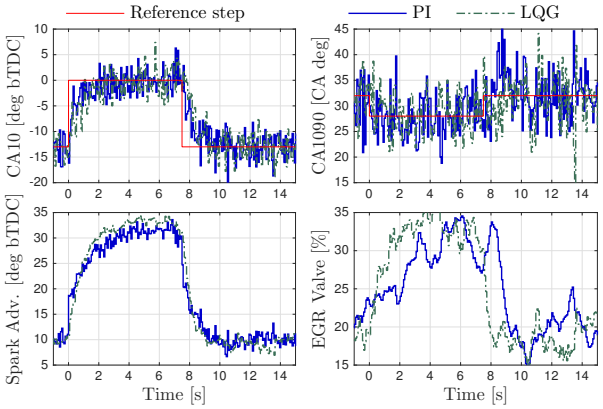

Fig. 7. Simulated comparison for step POINT B → POINT A → POINT B using the nonlinear model of Section III-C with measurement noise.

TABLE VI

SIMULATED STEP: POINT B → POINT A

CA10	Rise-time		Settling-time		Overshoot		Std. Dev.	
PI	1.88 [sec] 25 [cyc]	△	2.85 [sec] 38 [cyc]	△	0.00 0 %	⊙	2.30	○
LQG	1.95 [sec] 26 [cyc]	△	2.55 [sec] 34 [cyc]	△	0.05 0.40 %	⊙	2.28	○
CA1090	Rise-time		Settling-time		Overshoot		Std. Dev.	
PI	0.08 [sec] 1 [cyc]	⊙	4.05 [sec] 54 [cyc]	△	2.37 59.25 %	×	4.07	○
LQG	3.68 [sec] 49 [cyc]	×	4.50 [sec] 60 [cyc]	△	0.00 0 %	⊙	3.97	○

⊙: Very good △: Medium sec: Seconds
○: Good ×: Bad cyc: Cycles @ 1600 [RPM]

TABLE VII

SIMULATED STEP: POINT A → POINT B

CA10	Rise-time		Settling-time		Overshoot		Std. Dev.	
PI	1.50 [sec] 20 [cyc]	△	2.55 [sec] 34 [cyc]	△	0.00 0 %	⊙	2.65	○
LQG	1.50 [sec] 20 [cyc]	△	1.72 [sec] 23 [cyc]	○	0.00 0 %	⊙	2.54	○
CA1090	Rise-time		Settling-time		Overshoot		Std. Dev.	
PI	0.45 [sec] 6 [cyc]	⊙	3.45 [sec] 46 [cyc]	△	3.75 93.75 %	×	4.46	△
LQG	1.80 [sec] 24 [cyc]	△	1.88 [sec] 25 [cyc]	○	0.06 1.50 %	⊙	4.28	○

⊙: Very good △: Medium sec: Seconds
○: Good ×: Bad cyc: Cycles @ 1600 [RPM]

should remain unchanged. The LQG controller can achieve such time domain constrains for both outputs. Standard deviation at steady state indicates that closing the feedback loop will not increase considerably the combustion variability of the process as summarized in Tables VI and VII.

B. Frequency Domain

The LQG controller in Fig. 5 has the following control signal, disregarding disturbances and measurement noise:

$$U(z) = -C_{\text{LQG}}(z)Y(z) + C_{\text{ref}}(z)R(z) \tag{13}$$

where C_{LQG} corresponds to the feedback component [12]. On the other hand, the decentralized architecture in Fig. 4 is characterized by the feedback law:

$$U(z) = -C_{\text{PI}}(z)Y(z) = -\text{diag}\begin{pmatrix} PI_{SA} & PI_{EGR} \end{pmatrix} Y(z) \tag{14}$$

Figure 8 compares C_{PI} and C_{LQG} in frequency domain. Although the diagonal components are similar, the LQG controller avoids excessive overshoot due to the off-diagonal contribution. Fig. 9 shows the Bode magnitude plot of the

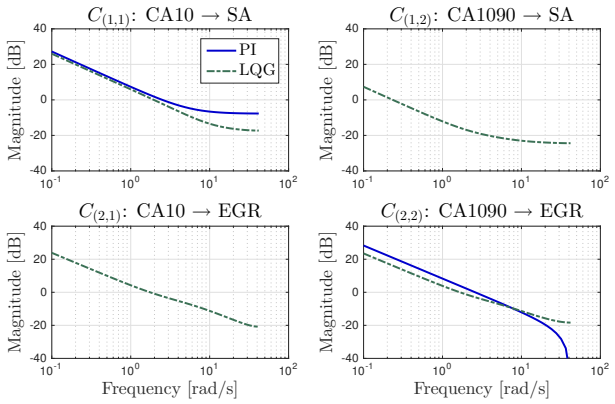

Fig. 8. Bode magnitude plot of feedback controller.

closed loop transfer function $T(z)$. Note that the bandwidth is similar for both controllers in the diagonal components. They also have an off-diagonal compensation in a similar band. However, the contribution of $C_{(2,1)}$ in the LQG controller reduces the $T_{(2,1)}$ interaction at all frequencies and hence avoids overly long combustion duration (overshoot) after the step change.

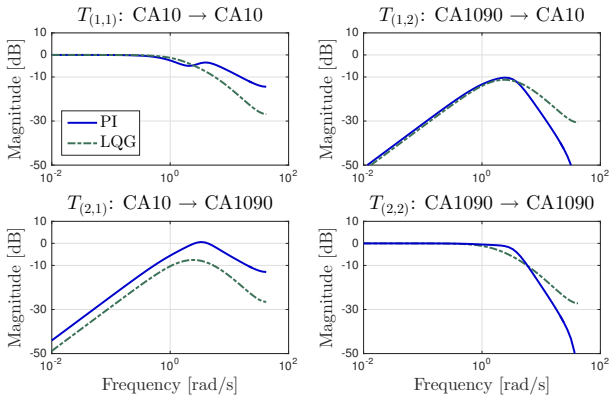

Fig. 9. Bode magnitude plot of closed loop system.

VII. CONCLUSIONS

Using an engine model derived from system identification, two different control architectures have been designed that drive combustion start and duration to desired set values using SA and EGR valve. Even though CV is present at all time the feedback loop did not increase measurement noise, maintaining the combustion within the normal operating range after the step command is performed. Comparison in time and frequency domains allows us to conclude that the LQG controller is beneficial because it coordinates SA and EGR commands to avoid overly long combustion durations that can cause misfires. Future work encompasses experimental validation of the engine response with the various feedback controllers and possible implementation of feedforward. Additional investigation will address the global behavior and transitions to operating points with different CV and dynamics.

ACKNOWLEDGMENT

We would like to thank Shigeyuki Urano, Yoshihiro Sakayanagi, and Junichi Kako of the Toyota Motor Corporation in addition to Masato Ehara and Dr. Ken Butts of Toyota Motor Engineering & Manufacturing North America for their invaluable input.

REFERENCES

[1] L. Eriksson and L. Nielsen, *Modeling and Control of Engines and Drivelines*, ser. Automotive Series. Wiley, 2014.

[2] R. J. Hosey and J. D. Powell, "Closed loop, knock adaptive spark timing control based on cylinder pressure," *Journal of Dynamic Systems, Measurement, and Control*, vol. 101, no. 1, pp. 64–69, 03 1979.

[3] L. Eriksson, "Spark advance modeling and control," Ph.D. dissertation, Division of Vehicular Systems, Department of Electrical Engineering, Linköping University, 1999.

[4] T. Alger, J. Gingrich, C. Roberts, and B. Mangold, "Cooled exhaust-gas recirculation for fuel economy and emissions improvement in gasoline engines," *International Journal of Engine Research*, vol. 12, no. 3, pp. 252–264, 2011.

[5] Z. Sun and G. G. Zhu, *Design and Control of Automotive Propulsion Systems*. CRC Press, 2015.

[6] J. D. Powell, "Engine control using cylinder pressure: Past, present, and future," *Journal of Dynamic Systems, Measurement, and Control*, vol. 115, no. 2B, pp. 343–350, 06 1993.

[7] T. Yamada, S. Adachi, K. Nakata, T. Kurauchi, and I. Takagi, "Economy with Superior Thermal Efficient Combustion (ESTEC)," in *SAE Technical Paper*. SAE International, 04 2014.

[8] A. Savitzky and M. J. E. Golay, "Smoothing and differentiation of data by simplified least squares procedures." *Analytical Chemistry*, vol. 36, no. 8, pp. 1627–1639, 07 1964.

[9] M. Morari, "Robust stability of systems with integral control," *IEEE Transactions on Automatic Control*, vol. 30, pp. 574–577, Jun 1985.

[10] E. Bristol, "On a new measure of interaction for multivariable process control," *IEEE Transactions on Automatic Control*, vol. 11, no. 1, pp. 133–134, Jan 1966.

[11] Y. Cao and D. Rossiter, "An input pre-screening technique for control structure selection," *Computers & Chemical Engineering*, vol. 21, no. 6, pp. 563 – 569, 1997.

[12] J. Freudenberg, "A first graduate course in feedback control," Winter 2016, unpublished lecture notes, The University of Michigan.

[13] C. J. Young, L. Jietae, J. J. Hak, L. Moonyong, and H. Chonghun, "Sequential loop closing identification of multivariable process models," *Computers & Chemical Engineering*, vol. 24, no. 2, pp. 809 – 814, 2000.

[14] G. Franklin, J. Powell, and M. Workman, *Digital control of dynamic systems*, ser. Addison-Wesley world student series. Addison Wesley Longman, 1998.